Multiscale Registration

Noémie Debroux, Carole Le Guyader, Luminita A Vese

Multiscale Registration*

Noémie Debroux[1], Carole Le Guyader[2]✉, and Luminita A. Vese[3]

[1] Université Clermont Auvergne, CNRS, SIGMA Clermont, Institut Pascal, F-63000 Clermont-Ferrand, France
noemie.debroux@uca.fr

[2] Normandie Univ, Institut National des Sciences Appliquées de Rouen, Laboratory of Mathematics, 76000 Rouen, France
carole.le-guyader@insa-rouen.fr

[3] Department of Mathematics, University of California Los Angeles, Hilgard Avenue, Los Angeles, CA 90095-1555, USA
lvese@math.ucla.edu

Abstract. In the seminal paper E. Tadmor, S. Nezzar and L. Vese, *A multiscale image representation using hierarchical* (BV, L^2) *decompositions*, Multiscale Model. Simul., 2(4), 554–579, (2004), the authors introduce a multiscale image decomposition model providing a hierarchical decomposition of a given image into the sum of scale-varying components. In line with this framework, we extend the approach to the case of registration, task which consists of mapping salient features of an image onto the corresponding ones in another, the underlying goal being to obtain such a kind of hierarchical decomposition of the deformation relating the two considered images (—from the coarser one that encodes the main structural/geometrical deformation, to the more refined one —). To achieve this goal, we introduce a functional minimisation problem in a hyperelasticity setting by viewing the shapes to be matched as Ogden materials. This approach is complemented by hard constraints on the L^∞-norm of both the Jacobian and its inverse, ensuring that the deformation is a bi-Lipschitz homeomorphism. Theoretical results emphasising the mathematical soundness of the model are provided, among which the existence of minimisers, a Γ-convergence result and an analysis of a suitable numerical algorithm, along with numerical simulations demonstrating the ability of the model to produce accurate hierarchical representations of deformations.

Keywords: Multiscale analysis · registration · nonlinear elasticity · Ogden materials · bi-Lipschitz homeomorphisms · Γ-convergence.

1 Introduction

Assuming that the considered grey-level images are L^2-observations that may include scale-varying objects, ranging from large homogeneous regions that are

* L. Vese acknowledges support from the National Science Foundation under Grant # 2012868. This project was co-financed by the European Union with the European regional development fund (ERDF, 18P03390/18E01750/18P02733) and by the Haute-Normandie Régional Council via the M2SINUM project.

faithfully modelled by the smaller functional space BV, to oscillatory patterns/ texture that require more involved functional spaces, multiscale representation can be viewed as the task which aims to accurately describe these different levels of details. This means representing the noticeable characteristics of a given image into suitable intermediate spaces/subclasses lying in between the rougher space L^2 (or L^p) and the smaller space BV of functions of bounded variation. While, as previously mentioned, this latter space is the proper one to describe homogeneous regions with sharp edges, finer details (whether it be oscillatory patterns or noise) are generally captured by a function or distribution belonging to a larger space such as L^p or a dual space of distributions (such as $\{\operatorname{div}\vec{g}\,|\,\vec{g}\in L^\infty\}$, $\{\operatorname{div}\vec{g}\,|\,\vec{g}\in \text{BMO (Bounded Mean Oscillation)}\}$ or $\{\Delta g\,|\,g \text{ Zygmund function}\}$, as suggested by Meyer ([11])). To identify such intermediate functional spaces, a standard strategy is interpolation (see [4] or [5]). The theory of interpolation studies the family of spaces Y that are intermediate spaces between Y_0 and Y_1, Banach spaces continuously embedded in the same Hausdorff topological vector space Z, in the sense that $Y_0 \cap Y_1 \subset Y \subset Y_0 + Y_1$. The model investigated in [24] falls within this framework and proves to be a special instance of the canonical form

$$J_p(f,\eta;X,Y) = \inf_{u+v=f} \{\|v\|_X^p + \eta\,\|u\|_Y\}$$

(closely related to the so-called K-functional (cf. [26, Chapter 5])) for which the intermediate spaces $(X,Y)_\theta$, $\theta\in[0,1]$ with $Y\subset X$, ranging from $(X,Y)_0 = X$ —the larger space —to $(X,Y)_1 = Y$ —the smaller one —are quantified by the behaviour of $J_p(\cdot,\eta;\cdot,\cdot)$ as η tends to 0. More precisely, in [24], the authors consider the larger functional space X to be L^2, while Y is chosen to be BV, and intend to measure how accurately an L^2-object can be approximated by its BV characteristics by considering the family of J-functionals

$$J(f,\lambda) = J_2(f,\lambda;BV,L^2) = \inf_{u+v=f} \left\{\lambda\,\|v\|_{L^2}^2 + \|u\|_{BV}\right\},$$

with increasing λ's. Note that the focus is shifted in comparison to the canonical form, from smaller η's to larger λ's.
The weighting parameter λ serves as a scale level to discriminate properly the two components: u, that captures the structural features of the observation f, while v encodes texture and oscillatory patterns, the discrimination between the two constituents being dictated by the scale parameter λ. This principle is embedded in a dyadic refinement process with λ_0 a given initial scale, that reads as:

$$\begin{aligned} &f = u_0 + v_0,\ \ [u_0,v_0] = \underset{u+v=f}{\arg\min}\ J(f,\lambda_0),\\ &v_j = u_{j+1} + v_{j+1},\ \ [u_{j+1},v_{j+1}] = \underset{u+v=v_j}{\arg\min}\ J(v_j,\lambda_0 2^{j+1}),\ j=0,1,\cdots, \end{aligned}$$

producing at the end of the k^{th} step, the following hierarchical decomposition:

$$f = u_0 + v_0 = u_0 + u_1 + v_1 = \cdots = u_0 + u_1 + \cdots + u_k + v_k,$$

the u_k's resolving finer edges. A remarkable result ([24, Theorem 2.2]) states that under the assumption $f \in BV$, the (BV, L^2) hierarchical decomposition of f, $\sum_{j=0}^{k} u_j$, strongly converges to f in L^2.
In accordance with this framework, we propose transposing it to the case of registration, the task which aims to determine an optimal (in a sense to be specified) diffeomorphic deformation φ that aligns the structures visible in an image called Reference into their counterparts in another one —called Template —(see [12, 13, 23] for a relevant analysis of the registration problem), the underlying goal being twofold: (i) obtaining a hierarchical decomposition of the sought deformation as $\varphi_0 \circ \cdots \varphi_k \circ \cdots \circ \varphi_n$, φ_0 encoding the main geometry-driven/structural deformation, while the $\varphi_0 \circ \cdots \circ \varphi_k$'s capture more refined deformations; (ii) assessing to what extent this hierarchical decomposition conveys the hidden structure of the deformation to be recovered, and how it could be used to derive image statistics, to measure variability inside a population, to retrieve the inherent dynamics of a phenomenon, and so on. The introduced algorithm is patterned after the one in [24] in the sense that it embeds successive applications of a refinement step —the composition of deformations is now a substitute for the sum of the scale-varying constituents of the seminal model [24] —, and can be schematised as follows. Given R (*resp.* T) the Reference (*resp.* Template) image and its related multilayered/hierarchical decomposition $\sum_{j=0}^{k} R_j$ (*resp.* $\sum_{j=0}^{k} T_j$), the algorithm reads as, $\mathcal{F}$ being a general functional that will be specified later on,

$$
\begin{aligned}
&\varphi_0 = \arg\min_{\varphi} \mathcal{F}(\varphi; R_0, T_0),\\
&\quad\vdots\\
&\varphi_k = \arg\min_{\varphi} \mathcal{F}(\varphi_0 \circ \cdots \circ \varphi_{k-1} \circ \varphi; \sum_{j=0}^{k} R_j, \sum_{j=0}^{k} T_j).
\end{aligned}
\tag{$\mathcal{D}$}
$$

Before depicting in depth our model, we would like to point out that prior related works ([17–19], [14]) suggest to foster the use of this image multiscale representation in a registration setting.
The work [17] is focused on (rigid) multiscale image registration for the registration of medical images degraded by significant levels of noise. Where conventional methods fail to correctly align the image pair, *i.e.*, to remove the artificial differences while highlighting the real differences due to intrinsic variations of the objects —whether it be ordinary registration techniques alone or sequential treatments including a prior step to denoise the image pair and then the application of a classical registration algorithm —, their proposed joint model achieves accurate registration. Given f an image with hierarchical expansion $\sum_{j=0}^{k} u_j$ —recall that for small k, $\sum_{j=0}^{k} u_j$ is a coarse representation of the image f that actually encodes the structural/geometrical information of f whilst removing small details —to be registered with g approximated by $\sum_{j=0}^{k} v_j$, the authors suggest registering the truncated hierarchical representations rather than f and g themselves, to get an accurate estimation of the deformation aligning them. Two main differences can be observed in comparison to our model: (i) first, each hierarchical step k is treated independently of the previous ones, that is, without connecting the optimal deformations $\Phi_0, \cdots, \Phi_{k-1}$ obtained at previous steps and the optimal deformation Φ_k produced at step k, whereas in

our approach, motivated by physical arguments stated below, deformation Φ_k is built up by taking advantage of the $\Phi_0, \cdots, \Phi_{k-1}$'s; (ii) second, and this is in some way a corollary of the first point, the optimal deformation Φ meant to bring f and g into spatial alignment is computed as a weighted average of the form $\frac{1}{m}\sum_{l=0}^{m-1} b_l\Phi_l$, the b_l's being weights appropriately chosen, while we promote composition of deformations. This work is then extended to the case of landmark-driven registration ([18]) in a B-spline setting and then, to the case of non-rigid deformations ([19]). The main motivation in our work to promote composition of deformations stems from the following fact stated in [25]. As mapping a point through a first transformation and then through a second one is equivalent to mapping the point through the composition of these two spatial transformations, the most natural and geometrically meaningful operation the space of non-parametric spatial transformations can be endowed with, is the composition. Note, on the contrary, that addition of spatial transformations has no geometric meaning.

More recently in [14], Modin *et al.* propose constructing analogous hierarchical expansions for diffeomorphims, the sum being replaced by composition of maps, in the context of image registration. Their method can be seen as a series of Large Deformation Diffeomorphic Metric Mapping (LDDMM) steps with varying weighting parameters (note that the adjective multiscale applies more to the way these weighting parameters are set at each iteration, *i.e.*, on how strong penalisations on the data fidelity term and on the deviation of the deformation composition from the identity mapping are, since they do not exploit the multiscale expansions of the images contrary to us). Although our method and theirs have in common the composition of deformations to refine the registration process, there are several key differentiating points in addition to the above: among them, the deformation model we embrace to describe the setting in which the objects to be matched are interpreted and viewed. In our case, it originates from physical considerations (*i.e.* elastic models in which the shapes to be matched are considered as the observations of a same body before and after being subjected to constraints) contrary to the model developed by Modin *et al.* which, to our point of view, is rather rooted in pure mathematical considerations and disconnected in some way from the physics of the problem. This choice of devising a model connected to physical considerations and especially to the hyperelasticity framework was motivated by the fact that it proves to be suitable when dealing with large and nonlinear deformations and that many applied problems, *e.g.* biological tissue behaviour, are modelled within this setting.

In [10], the authors propose decomposing the transformation f of the domain $D \subset \mathbb{R}^2$ in which the object is embedded, using quasi-conformal theories. As a desirable one-to-one representation of an orientation-preserving mapping $f : D \to D$ can be achieved via its Beltrami Coefficient (BC) $\mu(f) : D \to \mathbb{C}$ (—measure of non conformality, *i.e.*, to what extent a deformation deviates from a conformal map, and uniquely related to f by $\mu(f)(z) = \left(\frac{\partial f}{\partial \bar{z}}\right) / \left(\frac{\partial f}{\partial z}\right)$ —), the authors suggest applying a wavelet transform to the Beltrami coefficient, yielding a decomposition of the BC into different components of different frequencies compactly

supported in different sub-domains. Quasi-conformal mappings related to different components of the BC (different scales) can thus be reconstructed, those yielding a multiscale decomposition of the deformation.
Finally and for the sake of completeness, we refer the reader to [2], [9], [20] and [22] for alternative approaches.
We now turn to the mathematical formulation and analysis of the proposed physics-based multiscale modelling. We would like to point out that the core of the paper is on the fine theoretical properties exhibited by our modelling. The proofs being long, we have deliberately chosen to focus primarily on the asymptotic result, which, in our view, is the most significant one. A section is dedicated to the design of a suitable algorithm, but this does not constitute the crux of the manuscript. Extensive numerical simulations are currently being carried out to put this mathematical model to the test, and to assess its ability to unveil the hidden structure of the deformation to be retrieved.

2 Mathematical Modelling

2.1 Depiction of the Model

Let Ω be a connected bounded open subset of $\mathbb{R}^2$ of class $\mathcal{C}^1$, thus satisfying the cone property. Let us denote by $R : \bar{\Omega} \to \mathbb{R}$ the reference image and by $T : \bar{\Omega} \to \mathbb{R}$ the Template image, assumed to belong to the functional space $BV(\Omega)$. For theoretical and numerical purposes, we assume that T is compactly supported on Ω to ensure that $T \circ \varphi$ is always well-defined. Of course, in practice, the sought deformation should be with values in $\bar{\Omega}$, but from a mathematical point of view, if we work with such spaces, we lose the structure of vector spaces. Nonetheless, we can show that our model retrieves deformations with values in $\bar{\Omega}$ —based on Ball's results [3]. A deformation is a smooth mapping that is orientation-preserving and injective, except possibly on $\partial\Omega$. The deformation gradient is $\nabla\varphi : \bar{\Omega} \to M_2(\mathbb{R})$, the set $M_2(\mathbb{R})$ being the set of real square matrices of order 2. The sought deformation is seen as an argument of minimum of a specifically designed cost function comprising a regularisation on φ prescribing the nature of the deformation, and a term measuring alignment, or how the available data are used to drive the registration process. To allow large deformations, the shapes to be matched are viewed as isotropic (exhibiting the same mechanical properties in each direction), homogeneous (showing the same behaviour everywhere inside the material), hyperelastic materials (they exhibit both nonlinear behaviour and large changes in shape), and more precisely, as Ogden ones. Note that rubber, filled elastomers and biological tissues are often modelled within the hyperelastic framework, which motivates our approach. This perspective dictates the way the regularisation on the deformation φ is devised, based on the stored energy function of an Ogden material. Recall that the general expression of the stored energy function of such a material (see [6]) is given by $W_O(F) = \sum_{i=1}^{K} a_i \|F\|^{\gamma_i} + \Gamma(\det F)$, with $\forall i \in \{1, \cdots, K\}$, $a_i > 0$, $\gamma_i \geq 0$, and $\Gamma :]0, +\infty[\to \mathbb{R}$, being a convex function satisfying $\lim_{\delta \to 0^+} \Gamma(\delta) = \lim_{\delta \to +\infty} \Gamma(\delta) = +\infty$. The first term penalises changes in length, while the second one restricts the changes in area.

The latter one also ensures preservation of topology by enforcing positivity of the Jacobian almost everywhere. In this work, we focus more specifically on the following energy, $\|\cdot\|$ denoting the Frobenius norm,

$$W_{Op}(F) = \begin{cases} a_1\|F\|^4 + a_2(\det F - 1)^2 + \frac{a_3}{(\det F)^{10}} - 4a_1 - a_3 & \text{if } \det F > 0 \\ +\infty & \text{otherwise,} \end{cases}$$

which fulfils the previous assumptions. The two latter terms govern the distribution of the Jacobian determinant. While the middle term promotes Jacobian determinants close to 1, the rightmost one prevents singularities and large contractions by penalising small values of the determinant. The constants are added to comply with the energy property $W_{Op}(I) = 0$, where I stands for the identity matrix. In the following, we will set $W_{Op}(F) = \mathcal{W}_{Op}(F, \det F)$.
This stored energy function is complemented by the term $\mathbb{1}_{\{\|\cdot\|_{L^\infty(\Omega, M_2(\mathbb{R}))} \leq \alpha\}}(F)$ $+\mathbb{1}_{\{\|\cdot\|_{L^\infty(\Omega, M_2(\mathbb{R}))} \leq \beta\}}(F^{-1})$, with $\alpha \geq 1$, and $\beta \geq 1$, where $\mathbb{1}_A$ denotes the convex characteristic function of a convex set A, the underlying idea being to recover deformations that are bi-Lipschitz homeomorphisms.

Remark 1. In terms of functional spaces, if $\varphi \in W^{1,\infty}(\Omega, \mathbb{R}^2)$ (suitable space owing to the L^∞ hard constraints), $\det\nabla\varphi$ is automatically an element of $L^\infty(\Omega)$. Penalising the L^∞ norm of $\nabla\varphi$ thus entails control over the Jacobian determinant. This additional term implicitly gives an upper and lower bound on the Jabobian determinant ensuring thus topology preservation.

The aforementioned regulariser is then applied along with a classical L^2-discrepancy measure, yielding the following minimisation problem

$$\inf_{\varphi \in \mathcal{W}} \Big\{ F(\varphi) = \frac{\lambda}{2}\|T \circ \varphi - R\|^2_{L^2(\Omega)} + \int_\Omega \mathcal{W}_{Op}(\nabla\varphi, \det(\nabla\varphi))\, dx \qquad (\mathcal{P})$$
$$+ \mathbb{1}_{\{\|\cdot\|_{L^\infty(\Omega, M_2(\mathbb{R}))} \leq \alpha\}}(\nabla\varphi) + \mathbb{1}_{\{\|\cdot\|_{L^\infty(\Omega, M_2(\mathbb{R}))} \leq \beta\}}((\nabla\varphi)^{-1}) \Big\},$$

with $\mathcal{W} = \{\psi \in \mathrm{Id} + W^{1,\infty}_0(\Omega, \mathbb{R}^2) \mid \|\nabla\varphi\|_{L^\infty(\Omega, M_2(\mathbb{R}))} \leq \alpha,\ \|(\nabla\varphi)^{-1}\|_{L^\infty(\Omega, M_2(\mathbb{R}))} \leq \beta,\ \det(\nabla\varphi) > 0 \text{ a.e. in } \Omega\}$, and $\lambda > 0$.

2.2 Theoretical Results

The first theoretical result claims that problem $(\mathcal{P})$ admits at least one minimiser. Due to the limited number of pages, we only sketch the proof here.
Theorem 1. *Problem $(\mathcal{P})$ admits at least one minimiser in $\mathcal{W}$.*

Proof. The proof mainly relies on the following elements. Ball's results ([3]) enable one to conclude that any minimising sequence is such that $\forall k \in \mathbb{N}$, φ_k is a homeomorphism from Ω to Ω —and even from $\bar{\Omega}$ to $\bar{\Omega}$ owing to [3, Theorem 2]—, and more particularly, a bi-Lipschitz homeomorphism. Also, $\varphi_k \overset{*}{\underset{k\to+\infty}{\rightharpoonup}} \bar{\varphi}$ in $W^{1,\infty}(\Omega, \mathbb{R}^2)$ and similar arguments to those previously used enable one to

get that $\bar{\varphi}$ is a bi-Lipschitz homeomorphism from Ω to Ω and even from $\bar{\Omega}$ to $\bar{\Omega}$. By continuity of the trace operator, one gets that $\bar{\varphi} \in \mathrm{Id} + W_0^{1,\infty}(\Omega, \mathbb{R}^2)$. Now, φ_k^{-1} is uniformly bounded according to k in $W^{1,\infty}(\Omega, \mathbb{R}^2)$ using Poincaré-Wirtinger inequality, thus there exist a subsequence still denoted by φ_k^{-1} and $\bar{u} \in W^{1,\infty}(\Omega, \mathbb{R}^2)$ such that $\varphi_k^{-1} \underset{k\to+\infty}{\overset{*}{\rightharpoonup}} \bar{u}$ in $W^{1,\infty}(\Omega, \mathbb{R}^2)$. On the one hand, $\varphi_k^{-1} \circ \bar{\varphi} \underset{k\to+\infty}{\to} \mathrm{Id}$ in $L^\infty(\Omega, \mathbb{R}^2)$ due to the β-Lipschitz property of φ_k^{-1}, thus almost everywhere in Ω up to a subsequence. On the other hand, φ_k^{-1} uniformly converges to $\bar{u}$ in $\mathcal{C}^0(\bar{\Omega}, \mathbb{R}^2)$, yielding $\varphi_k^{-1} \circ \bar{\varphi} \underset{k\to+\infty}{\to} \bar{u} \circ \bar{\varphi}$ pointwise in $\bar{\Omega}$. By uniqueness of the limit, $\bar{u} \circ \bar{\varphi} = \mathrm{Id}$ a.e., leading to $\bar{u} = \bar{\varphi}^{-1}$ a.e. in Ω. It remains to address the question of weak lower semicontinuity. Since $T \in BV(\Omega)$ and all φ_k and $\bar{\varphi}$ are bi-Lipschitz homeomorphisms, we get that $\forall k \in \mathbb{N}$, $T \circ \varphi_k \in BV(\Omega) \subset L^2(\Omega)$ and $T \circ \bar{\varphi} \in BV(\Omega)$ (see [1, Theorem 2.6]). We then prove that $\varphi_k \circ \bar{\varphi}^{-1}$ strongly converges to Id in $\mathcal{C}^{0,\alpha}(\bar{\Omega}, \mathbb{R}^2)$, which is a cornerstone step to prove that $T \circ \varphi_k \underset{k\to+\infty}{\to} T \circ \bar{\varphi}$ in $L^2(\Omega)$.

We now include a multiscale representation of the deformation in our model, relying on the hierarchical decomposition into the sum of scale-varying components introduced in [24]. Let $(T_j)_j \in BV(\Omega)$ and $(R_j)_j \in BV(\Omega)$ be the sequence of varying scale structural features of respectively T and R coming from the following problems —S standing for either R or T below — :

$$\begin{cases} (S_0, v_0) &= \underset{(u,v)\in BV(\Omega)\times L^2(\Omega)\,|\,S=u+v}{\arg\min} \{\lambda_0 \|v\|_2^2 + TV(u)\}, \\ (S_{j+1}, v_{j+1}) &= \underset{(u,v)\in BV(\Omega)\times L^2(\Omega)\,|\,v_j=u+v}{\arg\min} \{2^{j+1}\lambda_0 \|v\|_2^2 + TV(u)\},\ j = 1, \ldots, \end{cases}$$

λ_0 being an initial scale parameter provided by the user. We refer the reader to [24] for a thorough description and analysis of this multiscale representation of an image.
In this work, we assume that T and R have similar scale structures and that each level of the following hierarchical decomposition of T, $\left(\sum_{j=0}^{k} T_j\right)$, can be matched to the corresponding level of hierarchical decomposition of R, $\left(\sum_{j=0}^{k} R_j\right)$. We then derive a corresponding hierarchical decomposition of the deformation, going from global structural deformations to more locally refined ones, and based on the composition operator —a more natural and physically meaningful operator than the addition for transformations —. This multiscale decomposition is described as follows :

$$\begin{cases} \varphi_0 = \underset{\varphi\in\mathcal{W}}{\arg\min}\{\mathcal{F}(\varphi, T_0, R_0)\}, \\ \varphi_k = \underset{\varphi\in\mathcal{X}_k}{\arg\min}\{\mathcal{F}(\varphi_0 \circ \varphi_1 \circ \ldots \circ \varphi_{k-1} \circ \varphi, \sum_{j=0}^{k} T_j, \sum_{j=0}^{k} R_j)\}, \end{cases} \qquad (\mathcal{P}_k)$$

with

$$\mathcal{F}(\varphi, T, R) = \frac{\lambda}{2}\|T \circ \varphi - R\|^2_{L^2(\Omega)} + \int_\Omega \mathcal{W}_{Op}(\nabla\varphi, \det(\nabla\varphi))\, dx + \mathbb{1}_{\{\|\cdot\|_{L^\infty(\Omega, M_2(\mathbb{R}))} \leq \alpha\}}(\nabla\varphi) + \mathbb{1}_{\{\|\cdot\|_{L^\infty(\Omega, M_2(\mathbb{R}))} \leq \beta\}}((\nabla\varphi)^{-1}),$$

and $\mathcal{X}_k = \{\psi \in \mathrm{Id} + W_0^{1,\infty}(\Omega, \mathbb{R}^2) \,|\, \det\nabla\psi > 0\, a.e., \, (\nabla(\varphi_0 \circ \varphi_1 \circ \ldots \circ \varphi_{k-1} \circ \psi))^{-1} \in L^\infty(\Omega, M_2(\mathbb{R}))\}$. The next theoretical result is a Γ-convergence result.

Theorem 2. *Problem ($\mathcal{P}_k$) admits at least one minimiser and the associated functional Γ-converges to the functional related to problem ($\mathcal{P}$) according to De Giorgi's definition.*

Proof. For the existence of minimisers, the same arguments as those previously used can be applied since orientation-preserving bi-Lipschitz homeomorphisms form a group stable for the composition, and $BV(\Omega)$ is stable for the sum. The Γ-convergence result mainly relies on [24, Theorem 2.2] stating the strong convergence of hierarchical decompositions to the initial image in $L^2(\Omega)$, as well as Ball's results [3]. These enable one to prove both inequalities required for the Γ-convergence property.

This result ensures that our multiscale decomposition gives a sequence of bi-Lipschitz homeomorphic deformations which model more and more locally refined distortions until it resembles the original deformation that maps T to R. We now turn to the numerical resolution of our problem ($\mathcal{P}_k$).

3 Numerical Resolution

Due to its non-linearity in both φ and $\nabla\varphi$ and its non-differentiability, problem ($\mathcal{P}_k$) is hard to solve numerically. Inspired by a prior work by Negrón Marrero [15] followed by more related works [16, 7, 8] in which the proposed numerical method is adapted to the image registration problem in a nonlinear elasticity setting, we introduce auxiliary variables with quadratic penalty terms. Especially, this enables us to decouple the deformation Jacobian from the deformation itself and from its inverse. For the sake of conciseness, we denote by $\bar{T}_k = \sum_{j=0}^{k} T_j$ and by $\bar{R}_k = \sum_{j=0}^{k} R_j$. The decoupled problem is thus defined by :

$$\begin{aligned}\inf_{\varphi,\psi,\phi,V,W} \mathcal{F}_k = {} & \tfrac{\lambda}{2}\textstyle\int_\Omega (\bar{T}_k \circ \phi - \bar{R}_k)^2\, dx + \int_\Omega W_{Op}(V, \det V)\, dx \\ & + \mathbb{1}_{\{\|\cdot\|_{L^\infty(\Omega, M_2(\mathbb{R}))} \leq \alpha\}}(V) + \mathbb{1}_{\{\|\cdot\|_{L^\infty(\Omega, M_2(\mathbb{R}))} \leq \beta\}}(W) \\ & + \tfrac{\gamma_1}{2}\|V - \nabla\phi\|^2_{L^2(\Omega, M_2(\mathbb{R}))} + \tfrac{\gamma_2}{2}\|W - \nabla\psi\|^2_{L^2(\Omega, M_2(\mathbb{R}))} \\ & + \tfrac{\gamma_3}{2}\|\zeta_{k-1}^{-1} \circ \phi - \varphi\|^2_{L^2(\Omega, \mathbb{R}^2)} + \tfrac{\gamma_4}{2}\|\psi \circ \phi - \mathrm{Id}\|^2_{L^2(\Omega, \mathbb{R}^2)}\end{aligned}, \qquad (\mathcal{P}_{k,d})$$

in which ϕ simulates $\varphi_0 \circ \varphi_1 \circ \ldots \circ \varphi_{k-1} \circ \varphi = \zeta_{k-1} \circ \varphi$, V mimics $\nabla\phi$ while W simulates $\nabla(\phi^{-1})$, and ψ approximates ϕ^{-1}. To design the L^∞-bound on

W, we used the fact that if u is a homeomorphism of Ω into Ω, and the inverse function u^{-1} belongs to $W^{1,q}(\Omega)$, the matrix of weak derivatives reads $\nabla(u^{-1}) = (\nabla u)^{-1}(u^{-1})$.
We then use a classical alternative scheme which consists of splitting the original problem into sub-problems that are more computationally tractable. The sketch of our numerical method of resolution is summarised in Algorithm 1. We now present numerical simulations validating the accuracy of the multiscale representation of the obtained deformation.

4 Numerical Experiments

We tested our model on 4DMRI[4] acquired during free-breathing of right lobe liver [21]. We chose the images (195×166) corresponding to the liver in full exhalation and the liver in full inhalation to illustrate the capability of our model to handle large deformations. The parameters were chosen as follows : $N = 10$ levels, $\lambda = 1$, $a_1 = 5.0$, $a_2 = 1000.0$, $a_3 = 4.0$, $\gamma_1 = 80000$, $\gamma_2 = 1.0$, $\gamma_3 = 1.0$, $\gamma_4 = 1.0$, $\alpha = 100$, and $\beta = 100$. The coefficients a_1, a_2 and a_3 involved in the Ogden stored energy function affect respectively the averaged local change of length, and the averaged local change of area. This leads to the following phenomenon: the higher the a_i's are, the more rigid the deformation is. The γ_i are chosen rather big to ensure the closeness between the auxiliary variables and the original ones. The λ weighs the fidelity term, and a trade-off has to be met between the accuracy of the registration with high values of λ and physically meaningful smooth deformations with small λ. The obtained results are illustrated in Fig.1.

We remark that for each level, the deformed Template is well-aligned with the Reference, demonstrating the ability of our model to deal with large deformations and localised small feature movements as the scale grows. The deformation grids do not exhibit overlaps and hence show that the obtained transformations are physically meaningful with a determinant remaining positive everywhere at all scales. By looking at the last column, one can see that the hierarchical decomposition of the deformations obtained with our model behaves as expected, that is to say the deformations on the first scales are global and represent the movements of the main organs and as k grows, the deformation becomes more localised and more refined to model the movements of small features, i.e. blood vessels imaged as small white dots.

5 Conclusion

To conclude, we have introduced a mathematically sound and physically relevant multiscale registration model inspired by the hierarchical decomposition presented in [24]. It shows promising results on medical data, producing deformations from global coarse deformations to localised finer transformations

[4] http://www.vision.ee.ethz.ch/ organmot/chapter_download.shtml

Algorithm 1 Our Proposed Method (L^∞ constraints applied componentwise)

Start from $\phi_{-1} \leftarrow \mathrm{Id}$, $V_{11,-1} \leftarrow 1$, $V_{12,-1} \leftarrow 0$, $V_{21,-1} \leftarrow 0$, $V_{22,-1} \leftarrow 1$, $W_{11,-1} \leftarrow 1$, $W_{12,-1} \leftarrow 0$, $W_{21,-1} \leftarrow 0$, $W_{22,-1} \leftarrow 1$ $\psi_{-1} \leftarrow \mathrm{Id}$, $\varphi_{-1} \leftarrow \mathrm{Id}$, and $\zeta_{-1} \leftarrow \mathrm{Id}$;
Choose N, the number of scales.
Compute $(T_j)_{j=0,\dots,N}$ and $(R_j)_{j=0,\dots,N}$;
for $k = 0, \dots, N$:
  $\bar{T}_k \leftarrow \sum_{j=0}^{k} T_j$, and $\bar{R}_k \leftarrow \sum_{j=0}^{k} R_j$;
  $\phi_k \leftarrow \phi_{k-1}$, $V_{11,k} \leftarrow V_{11,k-1}$, $V_{12,k} \leftarrow V_{12,k-1}$, $V_{21,k} \leftarrow V_{21,k-1}$, $V_{22,k} \leftarrow V_{22,k-1}$, $W_{11,k} \leftarrow W_{11,k-1}$, $W_{12,k} \leftarrow W_{12,k-1}$, $W_{21,k} \leftarrow W_{21,k-1}$, $W_{22,k} \leftarrow W_{22,k-1}$ $\psi_k \leftarrow \psi_{k-1}$, $\varphi_k \leftarrow \mathrm{Id}$, and $\zeta_{k-1} \leftarrow \phi_{k-1}$;
  for $l = 1, \dots, nbIter$:
    for each pixel :
      $V_{11,k} \leftarrow \mathrm{proj}_{\{\|.\|_{L^\infty(\Omega)} \leq \alpha\}}(V_{11,k} - (4\|V_k\|^2 V_{11,k} + 2a_2(\det V_k - 1) V_{22,k} - \frac{10a_3 V_{22,k}}{\det V_k^{11}} + \gamma_1(V_{11,k} - \frac{\partial \phi_{1,k}}{\partial x})))$;
      $V_{12,k} \leftarrow \mathrm{proj}_{\{\|.\|_{L^\infty(\Omega)} \leq \alpha\}}(V_{12,k} - (4\|V_k\|^2 V_{12,k} - 2a_2(\det V_k - 1) V_{21,k} + \frac{10a_3 V_{21,k}}{\det V_k^{11}} + \gamma_1(V_{12,k} - \frac{\partial \phi_{1,k}}{\partial y})))$;
      $V_{21,k} \leftarrow \mathrm{proj}_{\{\|.\|_{L^\infty(\Omega)} \leq \alpha\}}(V_{21,k} - (4\|V_k\|^2 V_{21,k} - 2a_2(\det V_k - 1) V_{12,k} + \frac{10a_3 V_{12,k}}{\det V_k^{11}} + \gamma_1(V_{21,k} - \frac{\partial \phi_{2,k}}{\partial x})))$;
      $V_{22,k} \leftarrow \mathrm{proj}_{\{\|.\|_{L^\infty(\Omega)} \leq \alpha\}}(V_{22,k} - (4\|V_k\|^2 V_{22,k} + 2a_2(\det V_k - 1) V_{11,k} - \frac{10a_3 V_{11,k}}{\det V_k^{22}} + \gamma_1(V_{22,k} - \frac{\partial \phi_{2,k}}{\partial y})))$;
      $W_{11,k} \leftarrow \mathrm{proj}_{\{\|.\|_{L^\infty(\Omega)} \leq \beta\}}(\frac{\partial \psi_{1,k}}{\partial x})$;
      $W_{12,k} \leftarrow \mathrm{proj}_{\{\|.\|_{L^\infty(\Omega)} \leq \beta\}}(\frac{\partial \psi_{1,k}}{\partial y})$;
      $W_{21,k} \leftarrow \mathrm{proj}_{\{\|.\|_{L^\infty(\Omega)} \leq \beta\}}(\frac{\partial \psi_{2,k}}{\partial x})$;
      $W_{22,k} \leftarrow \mathrm{proj}_{\{\|.\|_{L^\infty(\Omega)} \leq \beta\}}(\frac{\partial \psi_{2,k}}{\partial y})$;
  for each pixel
    Solve the Euler-Lagrange equation with respect to ϕ_k using an L^2 gradient flow with implicit Euler time stepping;
    Solve the Euler-Lagrange equation with respect to ψ_k using an L^2 gradient flow with implicit Euler time stepping;
    $\varphi_k \leftarrow \zeta_{k-1}^{-1} \circ \phi_k$;
  return $\phi_k, \psi_k, V_{11,k}, V_{12,k}, V_{21,k}, V_{22,k}, W_{11,k}, W_{12,k}, W_{21,k}, W_{22,k}, \varphi_k, \bar{T}_k \circ \phi_k$;

at different levels. A theoretical analysis of our numerical scheme (asymptotic result) complemented by additional tests with adapting parameters constitute the next steps of our work, along with an extension to more involved fidelity terms and a discussion on the possible statistics unveiled by this hierarchical decomposition.

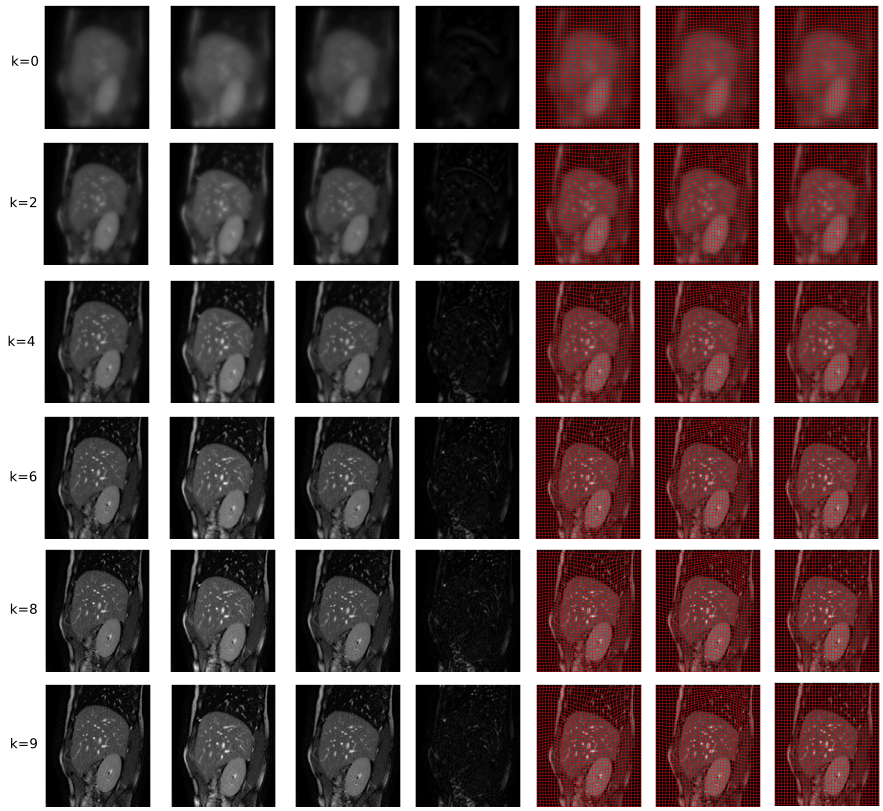

Fig. 1. Multiscale registration results : each row represents a scale of the deformation; the first column displays the Template image at scale k, i.e. $\bar{T}_k$, the second column shows the Reference image at scale k, i.e. $\bar{R}_k$, the third one illustrates the deformed Template obtained at scale k, i.e. $\bar{T}_k \circ \phi_k$, the fourth one exhibits the absolute difference $|\bar{T}_k \circ \varphi_k - \bar{R}_k|$ at scale k, the fifth column presents the inverse deformation at scale k, i.e. $\psi_k \approx \phi_k^{-1} \approx (\varphi_0 \circ \varphi_1 \circ \ldots \circ \varphi_k)^{-1}$, the sixth column represents the composition of deformations at scale k, i.e. $\phi_k \approx \varphi_0 \circ \varphi_1 \circ \ldots \circ \varphi_k$, and finally the last column displays the deformation obtained at scale k, i.e. φ_k.

References

1. Ambrosio, L., Bertrand, J.: DC calculus. Math. Zeitschrift **288**(3), 1037–1080 (2018)
2. Athavale, P., Xu, R., Radau, P., Nachman, A., Wright, G.A.: Multiscale properties of weighted total variation flow with applications to denoising and registration. Med. Image Anal. **23**(1), 28 – 42 (2015)
3. Ball, J.M.: Global invertibility of Sobolev functions and the interpenetration of matter. P. Roy. Soc. Edin. A **88**(3-4), 315–328 (1981)
4. Bennet, R., Sharpley, R.: Interpolation of Operators. Academic Press (1988)
5. Bergh, J., Löfström, J.: Interpolation Spaces. An Introduction. Springer, Berlin, Heidelberg (1976)

6. Ciarlet, P.: Elasticité Tridimensionnelle. Masson (1985)
7. Debroux, N., Le Guyader, C.: A joint segmentation/registration model based on a nonlocal characterization of weighted total variation and nonlocal shape descriptors. SIAM J. Imaging Sci. **11**(2), 957–990 (2018)
8. Debroux, N., Aston, J., Bonardi, F., Forbes, A., Le Guyader, C., Romanchikova, M., Schönlieb, C.B.: A variational model dedicated to joint segmentation, registration, and atlas generation for shape analysis. SIAM J. Imaging Sci. **13**(1), 351–380 (2020)
9. Gris, B., Durrleman, S., Trouvé, A.: A Sub-Riemannian Modular Framework for Diffeomorphism-Based Analysis of Shape Ensembles. SIAM J. Imaging Sci. **11**(1), 802–833 (2018)
10. Lam, K.C., Ng, T.C., Lui, L.M.: Multiscale Representation of Deformation via Beltrami Coefficients. Multiscale Model. Simul. **15**(2), 864–891 (2017)
11. Meyer, Y.: Oscillating Patterns in Image Processing and Nonlinear Evolution Equations: The Fifteenth Dean Jacqueline B. Lewis Memorial Lectures. American Mathematical Society (2001)
12. Modersitzki, J.: Numerical Methods for Image Registration. Oxford University Press (2004)
13. Modersitzki, J.: FAIR: Flexible Algorithms for Image Registration. SIAM (2009)
14. Modin, K., Nachman, A., Rondi, L.: A multiscale theory for image registration and nonlinear inverse problems. Adv. Math. **346**, 1009 – 1066 (2019)
15. Negrón Marrero, P.: A numerical method for detecting singular minimizers of multidimensional problems in nonlinear elasticity. Numer. Math. **58**, 135–144 (1990)
16. Ozeré, S., Gout, C., Le Guyader, C.: Joint segmentation/registration model by shape alignment via weighted total variation minimization and nonlinear elasticity. SIAM J. Imaging Sci. **8**(3), 1981–2020 (2015)
17. Paquin, D., Levy, D., Schreibmann, E., Xing, L.: Multiscale Image Registration. Math. Biosci. Eng. **3**(2), 389–418 (2006)
18. Paquin, D., Levy, D., Xing, L.: Hybrid multiscale landmark and deformable image registration. Math. Biosci. Eng. **4**(4), 711–737 (2007)
19. Paquin, D., Levy, D., Xing, L.: Multiscale deformable registration of noisy medical images. Math. Biosci. Eng. **5**(1), 125–144 (2008)
20. Risser, L., Vialard, F.X., Wolz, R., Murgasova, M., Holm, D.D., Rueckert, D.: Simultaneous Multi-scale Registration Using Large Deformation Diffeomorphic Metric Mapping. IEEE T. Med. Imaging **30**(10), 1746–1759 (2011)
21. von Siebenthal, M., Székely, G., Gamper, U., Boesiger, P., Lomax, A., Cattin, P.: 4D MR imaging of respiratory organ motion and its variability. Physics in Medicine & Biology **52**(6), 1547 (2007)
22. Sommer, S., Lauze, F., Nielsen, M., Pennec, X.: Sparse Multi-Scale Diffeomorphic Registration: The Kernel Bundle Framework. J. Math. Imaging Vis. **46**, 292–308 (2013)
23. Sotiras, A., Davatzikos, C., Paragios, N.: Deformable medical image registration: A survey. IEEE Trans. Med. Imaging **32**(7), 1153–1190 (2013)
24. Tadmor, E., Nezzar, S., Vese, L.: A Multiscale Image Representation Using Hierarchical (BV, L^2) Decompositions. Multiscale Model. Simul. **2**(4), 554–579 (2004)
25. Vercauteren, T., Pennec, X., Perchant, A., Ayache, N.: Diffeomorphic Demons: Efficient Non-parametric Image Registration. NeuroImage **45**, S61–72 (12 2008)
26. Vese, L., Le Guyader, C.: Variational Methods in Image Processing. Chapman & Hall/CRC Mathematical and Computational Imaging Sciences Series, Taylor & Francis (2015)